HOSTED BY

ELSEVIER

Available online at www.sciencedirect.com

ScienceDirect

Journal of Magnesium and Alloys 4 (2016) 295–301
www.elsevier.com/journals/journal-of-magnesium-and-alloys/2213-9567

Full Length Article

Experimental and numerical analyses of magnesium alloy hot workability

F. Abbassi [a,b,*], M. Srinivasan [a], C. Loganathan [c], R. Narayanasamy [d], M. Gupta [e]

[a] Mechanical Engineering Department, College of Engineering, Dhofar University, P.O. Box 2509, 211 Salalah, Oman
[b] URMSSDT, Ensit, University of Tunis, 5 Avenue Taha Hussein, BP, 56, Bâb Manara 1008, Tunisia
[c] Department of Mechanical Engineering, Chartered Institute of Technology, Abu Road, Sirohi, Rajasthan 307 510, India
[d] Department of Production Engineering, National Institute of Technology, Tiruchirappalli, Tamil Nadu 620 015, India
[e] Department of Mechanical Engineering, National University of Singapore, 9 Engineering Drive 1, Singapore 117 576, Singapore

Received 17 August 2016; revised 12 October 2016; accepted 15 October 2016

Available online 25 October 2016

Abstract

Due to their hexagonal crystal structure, magnesium alloys have relatively low workability at room temperature. In this study, the hot workability behavior of cast-extruded AZ31B magnesium alloy is studied through hot compression testing, numerical modeling and microstructural analyses. Hot deformation tests are performed at temperatures of 250 °C to 400 °C under strain rates of 0.01 to 1.0 s^{-1}. Transmission electron microscopy is used to reveal the presence of dynamic recrystallization (DRX), dynamic recovery (DRY), cracks and shear bands. To predict plastic instabilities during hot compression tests of AZ31B magnesium alloy, the authors use Johnson–Cook damage model in a 3D finite element simulation. The optimal hot workability of magnesium alloy is found at a temperature (T) of 400 °C and strain rate ($\dot{\varepsilon}$) of 0.01 s^{-1}. Stability is found at a lower strain rate, and instability is found at a higher strain rate.

Keywords: AZ31B magnesium alloy; Hot workability; Damage; Plastic instability; TEM analysis; FEM

1. Introduction

Magnesium based alloys are now the best candidate materials for structural applications owing to their light weight. This property renders magnesium alloys a good candidate for use in transportation industry applications such as spur bevel gears [1] and digital camera barrels [2] (Fig. 1). The superior workability of AZ31B magnesium alloy achieved at higher temperatures relative to that achieved at ambient temperatures has attracted the interest of researchers. Hot deformation involves the plastic deformation of materials formed at elevated temperatures without plastic instability. Deformation is affected by temperature, strain and strain rates. Hot deformation is dependent on extrinsic properties namely strain (ε), strain rates ($\dot{\varepsilon}$), work piece temperature and inherent material flow characteristics [3]. Hot workability analyses of various materials such as steel, aluminum and magnesium have been carried out using constitutive models and processing maps developed by Hu et al. [4] and Suresh et al. [5]. The hot workability of magnesium AZ31B alloy was established by Srinivasan et al. [6] using processing maps. Their study revealed DRX in the stability domain at temperature and strain rates of 350 to 400 °C and 0.1 to 0.01 s^{-1}, respectively.

In the present study, Johnson–Cook (J–C) model was used to predict the behavior of AZ31B during hot deformation. This model assumes thermal softening, strain rate hardening and strain hardening. The J–C model is used in a finite elements model of compression test of cast-extruded AZ31B samples while taking account the deterioration of mechanical characteristics through the application of a damage model. Transmission electron microscopy and macroscopic observations were performed to identify the occurrence of dynamic recrystallization dynamic recovery and plastic instability (cracks and shear bands).

2. Materials and processing

The material used in the present work was AZ31B, and its chemical composition is presented in Table 1 [7]. Ingots of AZ31B magnesium alloy (MGAL) were processed by disintegrated melt deposition at an alternative casting route. Ingots

* Corresponding author. College of Engineering, Dhofar University, P.O. Box 2509, Salalah 211, Oman. Fax. +968 23237777.
E-mail addresses: fethi@du.edu.om, abbassi.fethi1@gmail.com (F. Abbassi).

http://dx.doi.org/10.1016/j.jma.2016.10.004

(a) (b)

Fig. 1. Photos of magnesium alloy AZ31B applications: (a) spur bevel gear [1], (b) digital camera barrel [2].

were extruded at a temperature and extrusion ratio of 350 °C and 20:1, respectively. Extruded billets were formed into pieces of 15 mm in diameter and 15 mm in height with 0.8 mm diameter hole at mid-height for thermocouple insertion. Hole was provided to insert thermocouple that came into contact with the inner core of the extruded billets for measuring adiabatic temperature increases during hot deformation. Hot workability tests were conducted through uni-axial compression tests using a universal testing machine (make: FIE; model: UTES-10 servo-controlled) with a maximum load capacity of 100 kN and equipped with an environmental chamber. Specimen and die surface lubrications were carried out by spraying dry graphite before conducting the experiments. Very little barreling was observed as a result of the friction free lubricated surfaces prepared. All of the billets were water quenched after they were deformed up to true strain level of 0.5. Hot deformation tests were conducted at temperatures and strain rates of 250–400 °C and 0.01–1.0 s^{-1}, respectively.

The deformed billets were sliced at the center parallel to the compression axis. A transmission electron microscopy (TEM) metallographic examination was carried out on the polished cut-surface of the deformed specimens. The samples were ion-milled to perforation at an ion accelerating voltage of 3 kV on mechanically ground cut disks of less than 100 µm in thickness followed dimple grinding to less than 20 µm in thickness.

Table 1
Chemical composition (wt.%) of AZ31B magnesium alloy.

Al	Zn	Mn	Fe	Si	Cu	Ni	Mg
2.94	0.87	0.57	0.0027	0.0112	0.0008	0.0005	Bal.

3. Experimental results and discussion

Several experimental investigations were conducted to study the fracture mechanism of magnesium alloys [8,9] and behaviors during hot forming [10,11]. Fig. 2a shows the results of the test. Fig. 2b shows the macrostructure of the compressed test samples studied at three different temperatures (250, 300, and 400 °C) and at three strain rates (0.01, 0.1 and 1 s^{-1}) of magnesium alloy AZ31B. The figure shows characteristics of metal flow during hot compression. Surface cracking was sensitive to strain rates and occurred in the flow instability region within the temperature range. It is evident that no cracking occurred after the compression test, as the deformation temperature was higher than 400 °C at each strain rate. Cracking was observed in all of the test samples when the deformation temperature was lower than 250 °C. These results also denote that the appropriate forging temperature of AZ31B alloy should exceed 400 °C.

3.1. Hot deformation behavior

The true stress–strain curves presented in Fig. 3 were converted from load–displacement curves using the constant

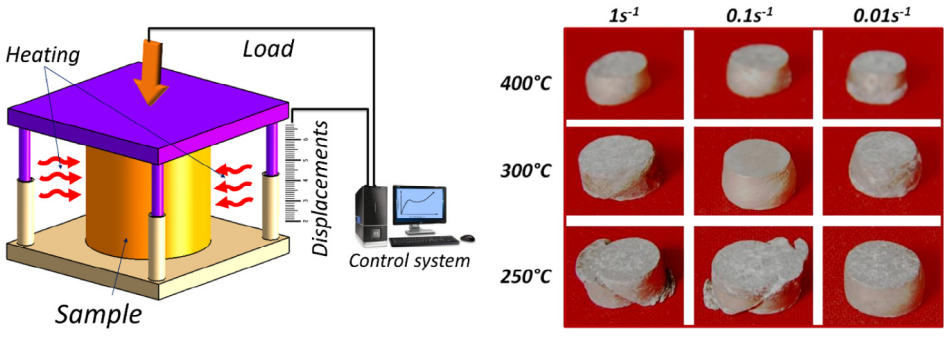

(a) (b)

Fig. 2. (a) Principal of compression test; (b) the specimens were deformed to a strain of about 0.5.

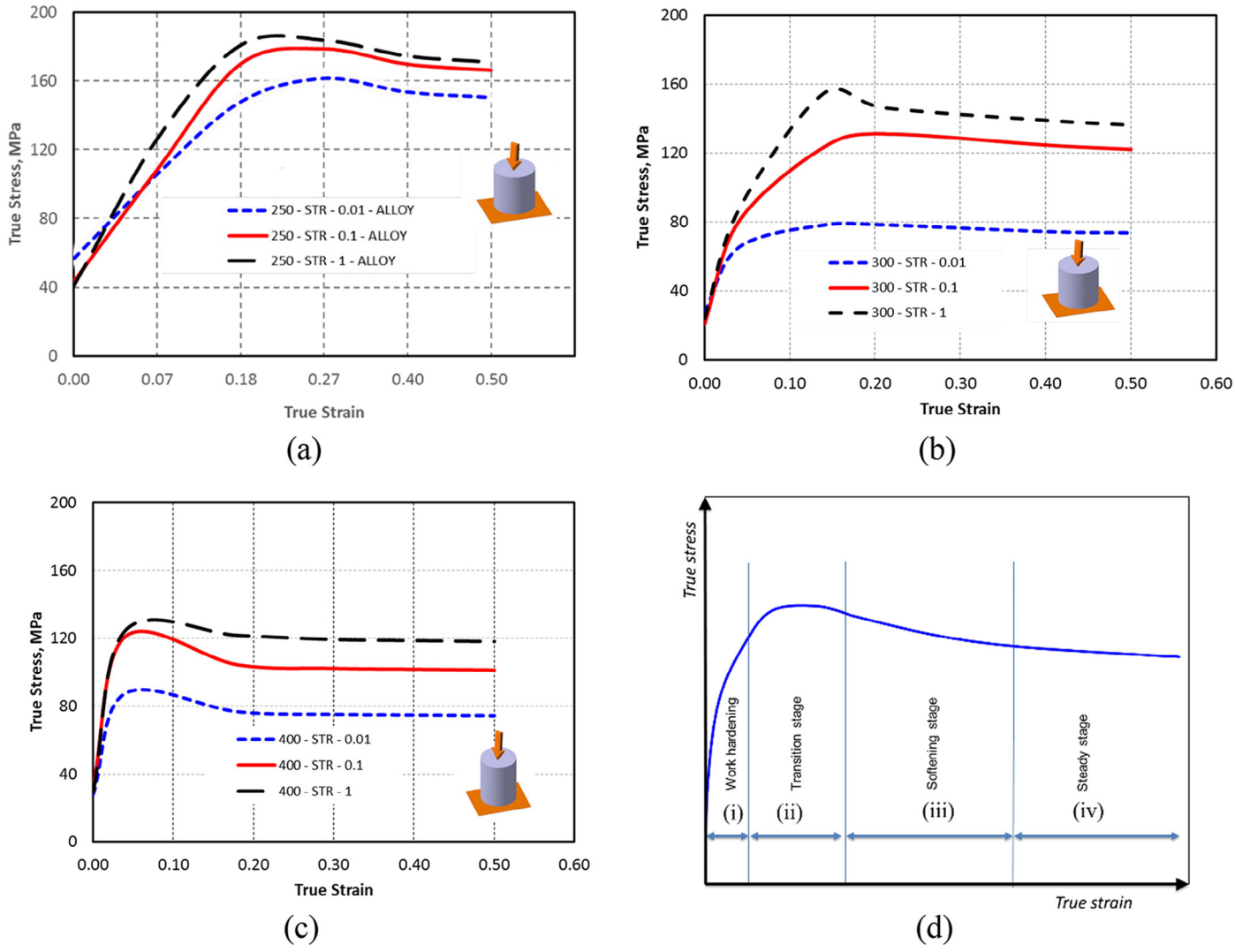

Fig. 3. The stress–strain curves of magnesium alloy AZ31B: (a) T = 200 °C, (b) T = 300 °C, (c) T = 400 °C, (d) typical true stress–strain behavior of the studied alloys under uniaxial compression.

volume assumption during axial compression tests [12]. In this stress–strain curve of magnesium alloys, four stages are commonly observed (Fig. 3d). These stages include (i) the work hardening stage, (ii) transition stage, (iii) softening stage and (iv) steady stage as reported by Shaha et al. [13], Qin et al. [14] and Jia et al. [15]. During stage (i), stress increases steeply with strain, stage (ii) represents competition between work hardening and softening phenomena. During stage (iii), according to dynamic recovery (DRY) and dynamic recrystallization (DRX) processes, stress levels drop steeply and localization phenomena cause instability viz. heating adiabatically and cracking. Finally, during stage (iv), at higher strain levels, stress levels stabilize. According to the flow curve, once the peak was reached, it exhibited flow softening at a lower strain rate (0.01 s^{-1}) and at strain levels of 0.1 to 0.25 followed by the onset of a steady state at 0.5. It is evident and in agreement with previous studies [16], at elevated temperatures and low strain rates the strain value of the peak is lower. According to these curves, we found that stress levels decrease with increasing deformation temperatures and decreasing strain rates.

3.2. Microstructural evolution

The magnesium alloy dynamic restoration method is highly susceptible to the chosen parameters and is strongly dependent on non-basal slippage throughout the hot working process. During hot compression, the dynamic restoration system viz. dynamic recrystallization (DRX) and dynamic recovery (DRY) occurs at a lower strain rate. Generally, power dissipation efficiency values of 35–45% and 20–30% correspond to DRX and DRY, respectively, based on dynamic material modeling [17] results. It is now evident from FE modeling based on the JC model that the domain may be related to DRX at an elevated temperature (400 °C) and at strain rates of 0.01–0.1 s^{-1}. The transmission electron microscopy image shown in Fig. 4 reveals the microstructure of the deformed specimen.

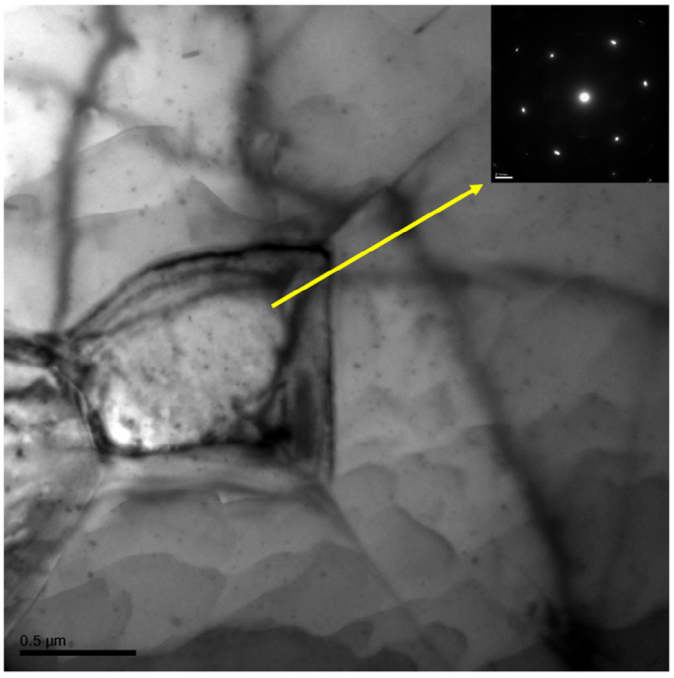

Fig. 4. Deformation at 400 °C/0.01 s^{-1} (insert selected area diffraction (SAD) confirms the absence of precipitates).

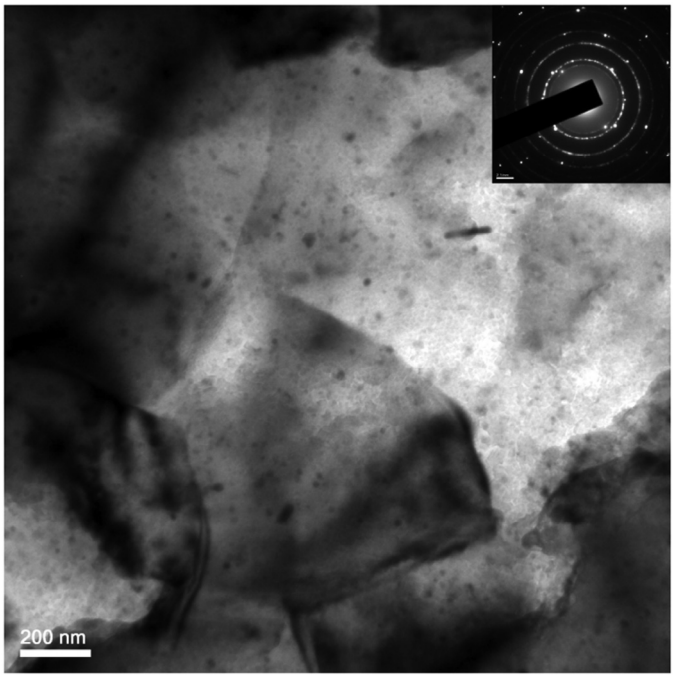

Fig. 5. Deformation at 300 °C/0.01 s^{-1} (insert selected area diffraction (SAD) confirms the presence of precipitates $Mg_{17}Al_{12}$).

The new recrystallized grain is found at higher workability temperatures and bulk recrystallization driving forces. At temperatures and strain rates of approximately 400 °C and 0.01 s^{-1}, respectively, DRX is observed. The TEM in Fig. 4 also shows refined grain and wavy grain boundaries. These denote the existence of DRX due to grain refinement in agreement with previous research [18]. Interface nucleation and interface grain growth rates are considered related to the occurrence of DRX as is shown in Fig. 4 in agreement with Raghunath et al. [19]. DRX is considered to be most favorable during hot working periods due to steady flows and safe effects on specimens as a result of concurrent softening and the presence of refined microstructures. Thus, hot workability is enhanced in this region.

The TEM image shown in Fig. 5 depicts the occurrence of dynamic recovery in AZ31B and the development of elongated grain in agreement with previous research [20,21]. This is clearly attributable to the development of elongated grain at a temperature range and lower strain rate of 250–300 °C and 0.1 s^{-1}, respectively.

It is evident from Fig. 6 and Fig. 7 that instabilities occurred at a strain rate range of 0.1–1.0 s^{-1}. Adiabatic shear bands, localized plastic flows and carking are probable causes of plastic instability. At a temperature and strain rate of 400 °C and 1.0 s^{-1}, respectively, the TEM image in Fig. 6 reveals the occurrence of dislocation bands and deformation twins. These instabilities are attributable to flow localization in the unstable region. This is in agreement with the available literature [22]. At a contained volume, deformation twins are immobile and cannot transmit the entire strain load. Here, deformation twins are susceptible to instigating cracks and contribute little to plasticity. At lower temperatures and as a result of shock loading, twins form in hexagonal close packing metals [23]. At higher strain rates or at lower temperatures, the formation of deformation twins and their orientation do not favor basal slippage in hcp metals. At low temperatures and high strain rates, flow localization is also observed as reported by Sivakesavam and Prasad [24].

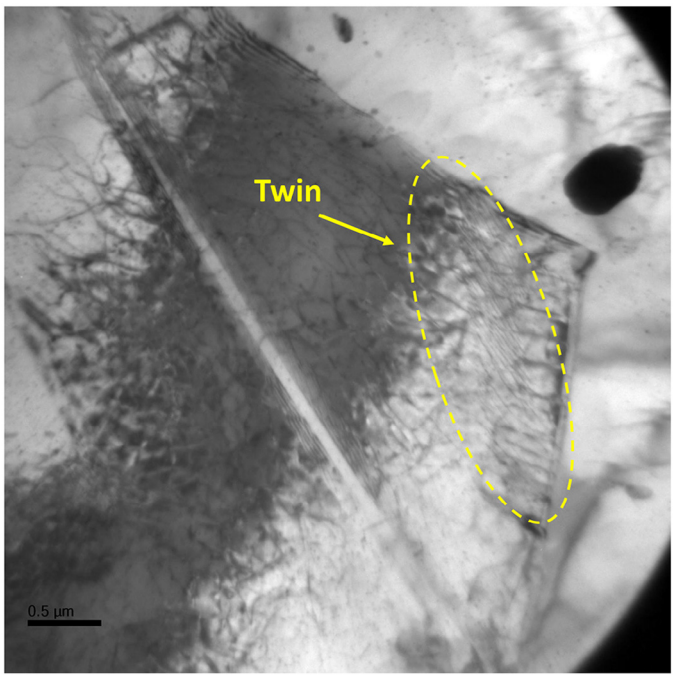

Fig. 6. Deformation at 400 °C and 1.0 s^{-1}.

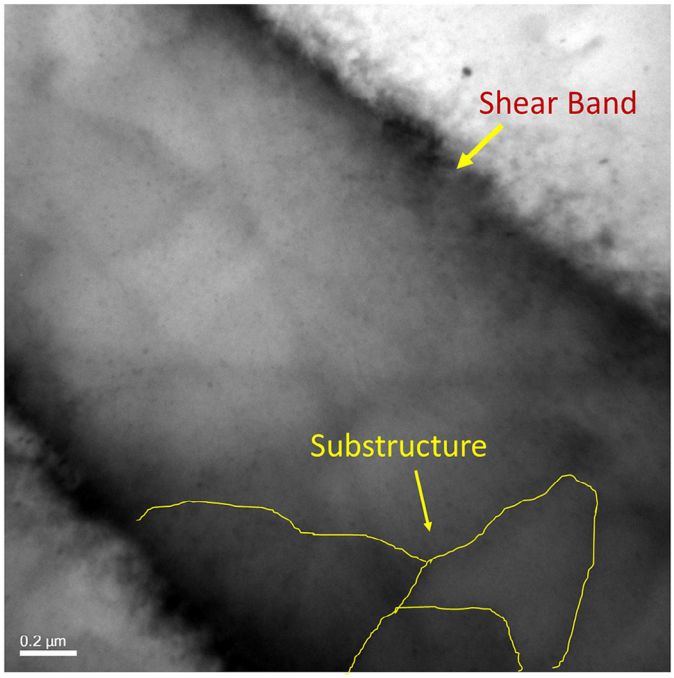

Fig. 7. Deformation at 300 °C and 1.0 s^{-1}.

Deformation due to shearing is observed in the shear band as shown in Fig. 7. Localized plastic flows occurred at a temperature and strain rate of 300 °C and 1.0 s^{-1}, respectively, in the deformed specimen as shown in Fig. 7. At high strain rates, the presence of cracking causes plastic instability. Similar observations are reported by Sivakesavam and Prasad [24] and Li et al. [25]. Severe adiabatic shear bands observed in the microstructure reveal cracking in the shear stress plane. Similar findings are reported by Anbuselvan and Ramanathan [26]. During hot deformation, heat produced as a result of localized temperatures may not be transferred to cooler specimens regions, as limited time is available at high strain rates as noted by Ramanathan et al. [27]. Deformation flow stress thus enhanced and nearly suited the adiabatic condition. Cracking patterns referred to as adiabatic shear bands were identified.

4. Numerical modeling

In recent years, several scholars have used processing maps to analyze the workability of materials, and especially for titanium and magnesium alloys. As such investigations of processing maps have only emphasized material properties, it is important to apply the finite elements method to simulate deformation and to predict the same phenomena [28], which appear during forming processes (e.g., damage and forming localization) as stated in Dong et al. [29].

4.1. Johnson–Cook models

The Johnson–Cook model (J–C) is one of many semi-empirical constitutive models that describe plastic material behaviors at high strain levels, strain rates and temperatures. The phenomenological constitutive relation proposed by Johnson–Cook to describe the flow stress can be expressed as [30]:

$$\sigma = \underbrace{(A + B\varepsilon^{n})}_{\text{quasi-static behavior}} \underbrace{\left[1 + C\ln\left(\frac{\dot{\varepsilon}}{\dot{\varepsilon}_0}\right)\right]}_{\text{Viscosity term}} \underbrace{\left[1 - T^{*m}\right]}_{\text{Thermal softening term}} \quad (1)$$

$$T^{*} = \frac{T - T_{room}}{T_{melt} - T_{room}} \quad (2)$$

where σ is material flow stress, ε is plastic strain, $\dot{\varepsilon}$ is the strain rate and $\dot{\varepsilon}_0$ is the reference strain rate. T is the temperature of the material, T_{melt} is the material melting point and T_{room} is the room temperature. The empirical constants are as follows: A is the yield stress, B is the increase in strength due to work hardening, C is the strain rate factor, n is the work-hardening exponent and m is the thermal softening exponent. Suppose that values of T_0 (20 °C) and ε_0 (0.01) are selected as quasi-static test conditions.

In addition to their basic model, Johnson and Cook presented a model for fracture prediction based on cumulative damage. The Johnson–Cook damage model is defined as [31]:

$$\varepsilon_f = \left[d_1 + d_2 \exp\left(-d_3 \frac{\sigma_m}{\sigma_e}\right)\right]\left[1 + d_4 \ln\left(\frac{\dot{\varepsilon}_e^{p}}{\dot{\varepsilon}_0}\right)\right]\left[1 + d_5 T^{*}\right] \quad (3)$$

where ε_f is the equivalent plastic fracture strain, σ^{*} is stress triaxiality which is the ratio of the pressure to the effective stress

$$\sigma^{*} = \frac{\mathrm{Pr}\,essure}{\bar{\sigma}} \quad (4)$$

d_1, d_2, d_3, d_4 and d_5 are fracture model constants obtained from experimentation.

As is shown by Dong et al. [29] and Jung et al. [32], damages to magnesium alloy during forming processes are sensitive to temperatures and strain rates, thus justifying the use of the Johnson–Cook damage model.

4.2. FE modeling of compression tests

Fig. 8 shows the FEM model of the hot compression process. The work piece is a ϕ12 × 12 mm cylinder that is considered a deformable solid, and top and bottom dies were considered as rigid plates. In his FE model, the Johnson–Cook model was used to describe the flow stress as a function of plastic strain, plastic strain rates and temperature. Table 2 shows the J–C parameters of AZ31B magnesium alloy [33]. Specimens were compressed to 50% of their original heights.

The numerical model results show that the deformation of the specimen was inhomogeneous, and the maximum degree of effective strain was found at the center of the specimen. Fig. 9 shows that the degree of the deformation inhomogeneity varies with forming temperature (T = 250 °C and 400 °C), stress and strain as is shown in Fig. 9 wherein the damage value reaches a value of 1 [34]. Fig. 10 shows the stress distribution on the compressed cylinder after 6 mm of displacement for different strain rate values.

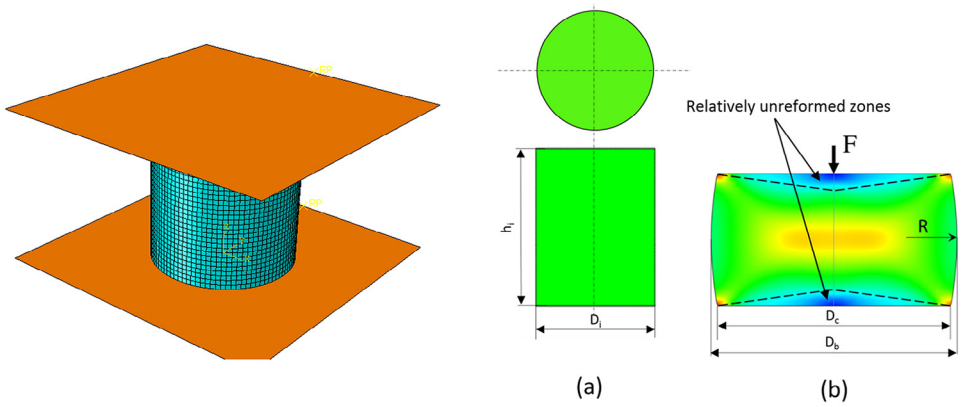

Fig. 8. Model of compression test, specimen before (a) and after (b) deformation.

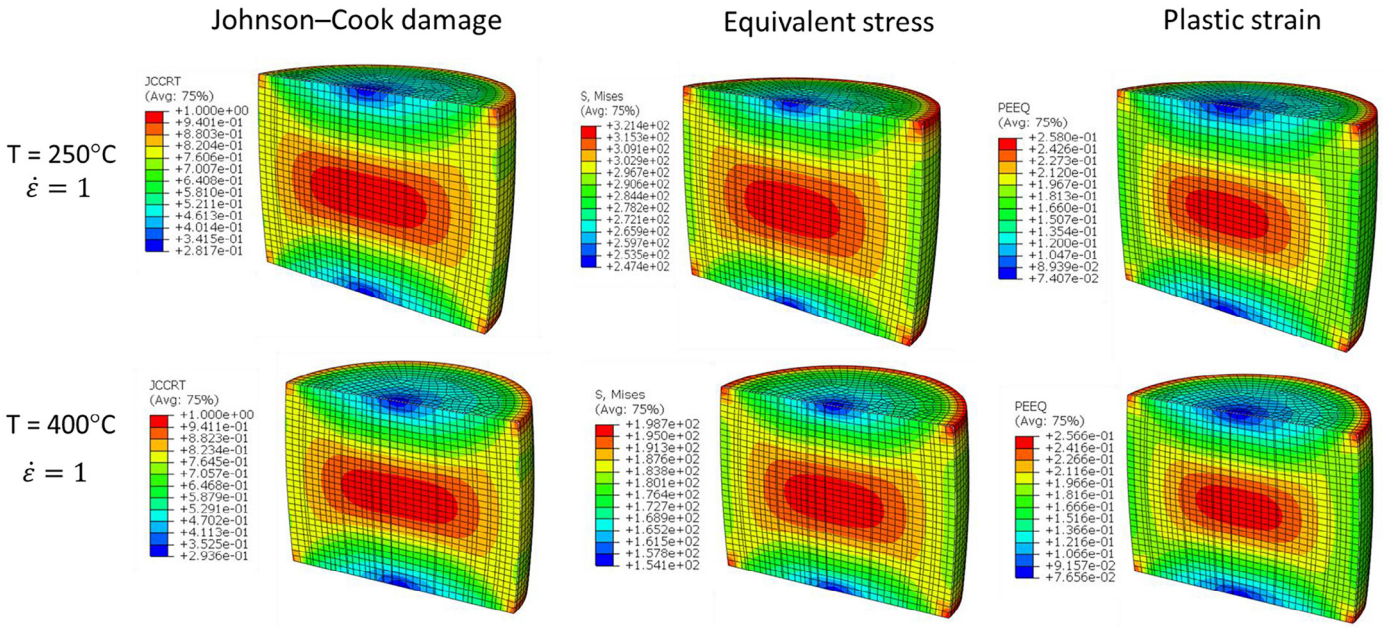

Fig. 9. Effect of forming temperature on workability and damage of formed parts (when the D = 1).

The hot workability of AZ31B magnesium alloy exhibits strong workability at a moderately higher temperature than room temperature, like other alloys with hexagonal close-packed structures. Thus, warm or hot forming is more favorable than cold forming.

Table 2
Material constant of the AZ31B magnesium alloy sheet [22].

AZ31B magnesium alloy parameters				
ρ (kg/m^3)	E (GPa)	ν	Yield stress (MPa)	
1780	45	0.34	172	
Constructive model parameters				
A (MPa)	B (MPa)	n	C	m
172	360.73	0.45592	0.092	0.95
Fracture model parameters				
d_1	d_2	d_3	d_4	d_5
−0.35	0.6025	−0.4537	0.206	7.2

5. Conclusions

The magnesium alloy AZ31B is sensitive to strain rates and temperatures, with grains coarsening under higher temperatures and over longer time periods. Plasticity levels rapidly decline with increasing strain rates.

- Our hot workability results for AZ31B alloy reveal that instability occurs when temperatures fall below 300 °C at all tested strain rates ranging from 0.01 to 1.0 s^{-1}.
- At elevated temperatures, the hot forming of this magnesium alloy shows instability viz. shear bands and deformation twins at a strain rate of 1.0 s^{-1}.
- We found high levels of AZ31B workability at a temperature of 400 °C and at a strain rate of 0.01 s^{-1}.
- DRX occurred at 400 °C and at a strain rate of 0.01 s^{-1} due to nucleation and grain growth according to TEM observations.

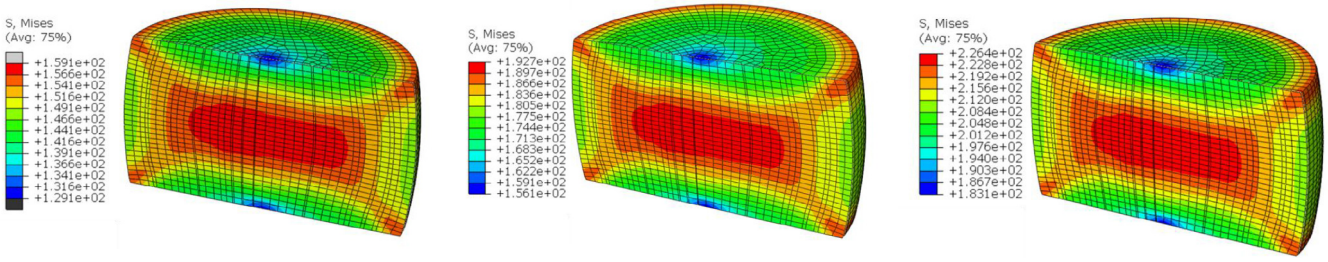

(a) strain rate ($\dot{\varepsilon}$) range of 0.01s-1 (b) strain rate ($\dot{\varepsilon}$) range of 0.01s-^{1}. (c) strain rate ($\dot{\varepsilon}$) range of 0.01s-^{1}.

Fig. 10. Effect of strain rate on von Mises stress distribution at temperature T = 400 °C (U = 6 mm).

- A numerical model that considers elastoplastic materials while taking into account damaging phenomena based on the Johnson–Cook extended model was developed.
- Our compression test simulation reveals estimations of specimen stress, strain, and damage evolution that complement our experimental findings.

References

[1] J. Liu, Z. Cui, J. Mater. Process. Technol. 209 (18–19) (2009) 5871–5880.
[2] C. Park, Y. Kim, Int. J. Precis. Eng. Manuf. 13 (7) (2012) 1047–1052.
[3] O. Grydin, M. Stolbchenko, F. Nürnberger, M. Schaper, J. Mater. Eng. Perform. 23 (3) (2014) 937–943.
[4] H.E. Hu, X.Y. Wang, L. Deng, Mater. Sci. Tech. 30 (11) (2014) 1321–1327.
[5] K. Suresh, C. Dharmendra, K.P. Rao, Y.V.R.K. Prasad, M. Gupta, Mater. Manuf. Process. 30 (10) (2015) 1161–1167.
[6] M. Srinivasan, C. Loganathan, R. Narayanasamy, V. Senthilkumar, Q.B. Nguyen, M. Gupta, et al., Mater. Des. 47 (2013) 449–455.
[7] Q.B. Nguyen, M. Gupta, J. Compos. Mater. 43 (2009) 5–17.
[8] M. Gzyl, R. Pesci, A. Rosochowski, S. Boczkal, L. Olejnik, J. Mater. Sci. 50 (6) (2015) 2532–2543.
[9] J. Shen, J. Shen, Y. Li, X. Xie, M. Liu, Mater. Manuf. Process. 29 (2) (2014) 188–193.
[10] S. Ucuncuoglu, A. Ekerim, G.O. Secgin, O. Duygulu, J. Magnes. Alloys 2 (1) (2014) 92–98.
[11] A. Hadadzadeh, M.A. Wells, J. Magnes. Alloys 1 (2) (2013) 101–114.
[12] S. Narayan, A. Rajeshkannan, Mater. Manuf. Process. 30 (10) (2015) 1196–1201.
[13] S.K. Shaha, F. Czerwinski, W. Kasprzak, D. Chen, J. Alloys Compd. 615 (2014) 1019–1031.
[14] Y.J. Qin, Q.L. Pan, Y.B. He, W.B. Li, X.Y. Liu, X. Fan, Mater. Manuf. Process. 25 (7) (2010) 539–545.
[15] W. Jia, S. Xu, Q. Le, L. Fu, L. Ma, Y. Tang, Mater. Des. 106 (2016) 120–132.
[16] M.R. Barnett, J Light Met 1 (2001) 167–177.
[17] N. Srinivasan, Y.V.R.K. Prasad, P. Rama Rao, Mater. Sci. Eng. 476 (1–2) (2008) 146–156.
[18] G. Jagan Reddy, N. Srinivasan, A.A. Gokhale, B.P. Kashyap, J. Mater. Process. Technol. 209 (18–19) (2009) 5964–5972.
[19] B.K. Raghunath, R. Karthikeyan, G. Ganesan, M. Gupta, Mater. Res. 9 (2006) 217–222.
[20] A. Momeni, K. Dehghani, Mater. Sci. Eng. 528 (3) (2011) 1448–1454.
[21] C.Y. Wang, K. Wu, M.Y. Zheng, Mater. Sci. Eng. 477 (1–2) (2008) 179–184.
[22] C.Y. Wang X., J. Wang, H. Chang, K. Wu, M.Y. Zheng, Mater. Sci. Eng. 464 (1–2) (2007) 52–58.
[23] G.E. Dieter, Mechanical Metallurgy, McGraw Hill Press, London, 1988.
[24] O. Sivakesavam, Y.V.R.K. Prasad, Mater. Sci. Eng. (2002) 270–277.
[25] A.B. Li, L.J. Huang, Q.Y. Meng, L. Geng, X.P. Cui, Mater. Des. 30 (5) (2009) 1625–1631.
[26] S. Anbuselvan, S. Ramanathan, Mater. Des. 31 (5) (2010) 2319–2323.
[27] S. Ramanathan, R. Karthikeyan, M. Gupta, J. Mater. Process. Technol. 183 (1) (2007) 104–110.
[28] L.J. Hu, Y.H. Peng, D.Y. Li, S.R. Zhang, Mater. Manuf. Process. 25 (8) (2010) 880–887.
[29] J.-R. Dong, D.-F. Zhang, Y.-F. Dong, F.-S. Pan, S.-S. Chai, Rare Metals (2015) 1–6.
[30] G. Johnson, W. Cook, Proc. 7th Int. Symp. on Ballistics, 1983.
[31] G.R. Johnson, W.H. Cook, Eng Fract Mech 21 (1) (1985) 31–48.
[32] K.H. Jung, Y.B. Kim, G.A. Lee, S. Lee, E.Z. Kim, D.S. Choi, Mater. Manuf. Process. 29 (2) (2014) 115–120.
[33] F. Feng, S. Huang, Z. Meng, J. Hu, Y. Lei, M. Zhou, et al., Mater. Sci. Eng. 594 (2014) 334–343.
[34] A. Zomorodian, M.P. Garcia, T. Moura e Silva, J.C. Fernandes, M.H. Fernandes, M.F. Montemor, Acta Biomater. 9 (10) (2013) 8660–8670.